frontiers | Frontiers in Earth Science

TYPE Original Research
PUBLISHED 12 October 2023
DOI 10.3389/feart.2023.1267211

OPEN ACCESS

EDITED BY
Lidong Dai,
Chinese Academy of Sciences, China

REVIEWED BY
Maining Ma,
University of Chinese Academy of Sciences, China
Xiaoge Huang,
Chinese Academy of Sciences (CAS), China
Chang Su,
Institute of Disaster Prevention, China

*CORRESPONDENCE
Haoran Zhang,
iggcaszhanghr@163.com
Xiwei Xu,
xiweixu@vip.sina.com

RECEIVED 26 July 2023
ACCEPTED 20 September 2023
PUBLISHED 12 October 2023

CITATION
Zhang H, Xu X and Yang S (2023), Ultramafic pseudotachylytes in high-pressure metamorphogenic peridotite from Luobusha, Tibet: a record of crustal paleo-earthquakes.
Front. Earth Sci. 11:1267211.
doi: 10.3389/feart.2023.1267211

Ultramafic pseudotachylytes in high-pressure metamorphogenic peridotite from Luobusha, Tibet: a record of crustal paleo-earthquakes

Haoran Zhang[1]*, Xiwei Xu[2]* and Saihong Yang[3]

[1]State Key Laboratory of Earthquake Dynamics, Institute of Geology, China Earthquake Administration, Beijing, China, [2]School of Earth Sciences and Resources, China University of Geosciences, Beijing, China, [3]Key Laboratory of Lunar and Deep Space Exploration, National Astronomical Observatories, Chinese Academy of Sciences, Beijing, China

In this paper, we report an occurrence of ultramafic pseudotachylytes, providing fault-rock evidence of paleo-earthquakes, from the Luobusha ophiolite complex in the Yarlung Zangbo suture zone. The pseudotachylytes form hairline-thin aphanitic veinlets and vein networks bounded by micro-damage zones cutting through the host harzburgite, forming flow banding in some places. The pseudotachylyte veins are dominated by close-knit ultrafine-grained minerals consisting of olivine, orthopyroxene, serpentine, spinel, and magnetite, cemented by an extremely fine matrix. As the primary component of the pseudotachylyte veins, olivine occurs as microphenocryst showing zoning from core to rim and as irregularly shaped microlite immersed in the interstitial material. Zoned crystals of olivine developed with Mg-rich cores and more Fe-rich rims. Microlite diagnosis of crystallization in a quenched melt includes dendritic, skeletal, and poikilitic olivine crystals, which are typical of ultramafic pseudotachylyte. The olivine microlites contain higher amounts of Ca, Al, and Cr but a lower Ni content compared with the host harzburgite olivine. Irregularly shaped chrome-spinel crystals are chemically zoned as well, indicating an Fe-rich rim overgrowth. Ni sulfide droplets interspersing among the matrix imply melt occurrence. The presence of a micro-fibrous and micro-vesicular interstitial matrix also indicates a melting-related origin. Ultracataclastite veins associated with pseudotachylyte transecting serpentine are observed, which convey that heat was generated during rapid comminution and injection. The characteristic petrography, microtextures, and chemical inhomogeneities meet the criteria of ultramafic pseudotachylyte and reveal a mixed genesis via a combination of crushing and melting. The development of extremely tiny globular prograde serpentine inclusions (~100 nm) in the olivine microlites is ascribed to the dehydration reaction of serpentine to olivine within the pseudotachylyte. The Luobusha metamorphogenic peridotite was subjected to serpentinization after having emplaced in the crust and subsequently to high-pressure metamorphism. The pseudotachylytes were generated in the crust after the high-pressure metamorphism and did not descend to a greater depth. Flash ultra-comminution associated with frictional heating may release fluids via localized heat-driven prograde reactions in the crust.

KEYWORDS

pseudotachylyte, quench, melt, dehydration, high-pressure metamorphism, Luobusha

1 Introduction

It is known that pseudotachylytes can be generated during earthquakes, meteoritic impacts, and large-scale landslides (Lin, 2008). Tectonogenetic pseudotachylytes that are related to seismic activities have generally been considered as products formed under the condition of high strain rates within shear zones and/or seismic fault zones (McKenzie and Brune, 1972; Sibson, 1975; Spray, 1987; 1995; Magloughlin, 1992; McNulty, 1995; Lin and Shimamoto, 1998). Frictional heating and strong abrasion that are generated during rapid seismic faulting are sufficient to melt and/or crush rock within the fault zone and fluidize ultrafine-grained materials (Kano et al., 2004), which eventually give rise to pseudotachylytes. More pseudotachylytes recognized from crustal sialic protoliths, such as crystalline rocks of intermediate and granitoid composition, have been reported in the literature, but cases of pseudotachylytes derived from peridotite are less common. The possible reasons why ultramafic pseudotachylyte has rarely been spotted are that peridotite is not a major constituent of the crust, its required melting temperatures are high, and its density inhibits uprise from great depths in the subduction zone (Evans and Cowan, 2012). However, the lower creep strength of silica-rich rocks compared with ultramafic rocks at the same melting temperatures would make it difficult to realize the high-stress conditions needed for frictional melting of silicic or basic rocks. In addition, the thermal feedback effect that may cause frictional melting may be easier for ultramafic rocks because of the higher activation energies of creep (Tullis and Yund, 1982; Karato, 1989). Hence, a relatively reasonable explanation for this scarcity of ultramafic pseudotachylyte is that evidence of possible ultramafic melts may be easily obscured by more rapid grain growth and recrystallization in ultramafic rocks than in silicic rocks (Karato, 1989). Research studies concerning ultramafic pseudotachylyte from the Balmuccia lherzolite, Ivrea–Verbano zone, North Italy, have demonstrated that shear heating can cause high-degree heating so that ultramafic rocks, which have a much higher melting temperature than other crustal rocks, undergo a significant degree of melting, followed by rapid crystallization on a time scale of 100 s or less, conditions consistent with an earthquake that may occur mainly in the oceanic upper mantle (Obata and Karato, 1995; Jin et al., 1998). Near-complete melting of peridotite took place during exhumation of the lithospheric mantle in the early stages of the formation of the Ligurian Tethys oceanic basin, which resulted in the formation of pseudotachylytes from the Mt. Moncuni ultramafic in the western Alps of Italy (Piccardo et al., 2010). Pseudotachylytes also developed in mantle peridotite at the Alpine subduction complex of Corsica during subduction-related faulting of metabasites and metaperidotites under lawsonite–blueschist facies conditions were described in detail (Austrheim and Andersen, 2004; Andersen and Austrheim, 2006; Andersen et al., 2008; Deseta et al., 2014). In the upper part of the Alpine subduction zone, frictional heating on co-seismic faults raised the temperature from ambient blueschist facies conditions to more than 1,700°C, which resulted in disequilibrium melting of spinel peridotite (Andersen and Austrheim, 2006).

The typical mineralogy and texture of most field examples of ultramafic pseudotachylyte reported to date have been generalized and summarized in detail, which could provide us much valuable references to aid the recognition of ultramafic pseudotachylyte. Moreover, a genetic association between co-seismic deformation and high-pressure metamorphism has been proposed and realized at some localities worldwide (Austrheim and Boundy, 1994; Austrheim et al., 1997; Lund and Austrheim, 2003; Austrheim and Andersen, 2004; John and Schenk, 2006; Angiboust et al., 2012; Austrheim, 2013; Andersen et al., 2014; Yang J.- et al., 2014; Yang et al., 2014 J.-J., 2016). It is considered that the role of faults or shear zones is to introduce a fluid that enhances metamorphic reactions at depths in the subducted slab through studies on eclogite pseudotachylyte that indicates fossil earthquake (Austrheim and Boundy, 1994; Austrheim, 2013). However, eclogite facies, such as breccia and cataclasite dykes, as well as the quench textures in a variably eclogitized gabbro at Yangkou in the Chinese Su-Lu ultrahigh-pressure metamorphic belt, are interpreted to be the result of co-seismic high-pressure metamorphism in the crust instead of high-pressure crystallization in subducted dry rocks when fluid becomes available (Yang J.- et al., 2014; Yang et al., 2014 J.-J., 2016). If the rocks were held at great depths for millions of years after the seismic events, then the quenching textures would have been erased owing to continuous mineral growth and equilibration in the stability of the eclogite (Yang J.-J. et al., 2014). In addition, the wall rock to the pseudotachylyte and associated ultracataclastite was subjected to serpentinization after having emplaced in the shallow crust and then transformed back into peridotite by subsequent high-pressure metamorphism (Huang et al., 2014). In several similar observations reported in the study of orogenic belts worldwide (Evans and Trommsdorff, 1978; Trommsdorff et al., 1998; Yang, 2003; Bucher, 2005; Ravna et al., 2006; Yang and Powell, 2008; Naemura et al., 2009; Morgunova and Perchuk, 2012; Rebay et al., 2012; Debret et al., 2013), it is proposed that a similar process may be experienced by all orogenic peridotites (Yang et al., 2013). Therefore, a research issue to be tackled is whether the earthquake in peridotite and associated high-pressure metamorphism occurred at mantle depth (Obata and Karato, 1995; Jin et al., 1998; Austrheim and Andersen, 2004), as has been assumed, or whether they took place in the brittle regime of the crust.

The present study documents some types of ultra-thin dark-brown aphanitic veinlets and vein networks occurring in harzburgite at the Luobusha ophiolite complex in the Yarlung Zangbo suture zone. The detailed petrographic observation shows that they are composed of fine- and ultrafine-grained minerals and take the form of tenuous branches parallel to or intersected with each other at small angles. The microtextures of these dark-brown veinlets obtained from scanning electron microscopy observation and their mineral chemistry are similar to some natural ultramafic pseudotachylytes described in previous papers (Obata and Karato, 1995; Andersen and Austrheim, 2006; Piccardo et al., 2010; Deseta et al., 2014) and to the run products generated during the high-velocity friction experiments (Lin et al., 2013), which make us fully convinced that these melanocratic veinlets are ultramafic pseudotachylyte formed in harzburgite at this locality. It is for the first time that ultramafic pseudotachylyte has been recognized in the Yarlung Zangbo suture zone. This study presents petrographic, microtextural, and mineral chemical data for the ultramafic pseudotachylyte at Luobusha. In addition, the ultramafic pseudotachylyte within the high-pressure metamorphogenic peridotite at this locality, thus, provides an opportunity to examine the interaction mechanism of co-seismic deformation and high-pressure metamorphism.

2 Geological setting

The Luobusha ophiolite (Figure 1) lies approximately 200 km southeast of Lhasa along the Yarlung Zangbo suture zone—a major tectonic boundary that separates the Lhasa Block to the north from the Indian plate to the south (Allégre et al., 1984). The ophiolite in this part of the suture zone extends for about 42 km in an east–west direction, with an outcrop area of approximately 70 square kilometers (Zhou et al., 1996; Robinson et al., 2004). The mantle peridotite mainly consists of harzburgite, in which there are a large number of dunite and podiform chromitite blocks, as well as a small amount of lherzolite, distributed in the southern ophiolite belt and in fault contact with the southern flysch formation (Zhang et al., 1996). According to the vertical variation of rock assemblage and chemical composition in the section sequence, the mantle peridotite can be divided into upper and lower subzones (Chen et al., 2011). The upper subzone is distinguished from other bodies in the Yarlung Zangbo ophiolite belt by the obvious increase of ductility (the main chromite metallogenic belt). In the strongly deformed peridotite, most dunite rocks are long, lenticular, and plate-like bodies with the same orientation and occurrence as the peridotite body. In addition, there are a few dunite rocks with various forms, weak directionality, and irregular boundaries, which form a sharp or gradual transition with harzburgite. The lower subzone is characterized by less dunite and more harzburgite, which is in a transitional relationship with the upper subzone. This zonation in the profile is considered to be a reflection of the zonation melting of the upper mantle rather than the result of magmatic differentiation (Chen et al., 2011). The cumulate rocks mainly include wehrlite, pyroxenite, dunite, and gabbro. To the south, the ophiolite underlies a thick sequence of Triassic flysch-type sedimentary rocks through a steep thrust fault; to the north, it thrusts over the Gangdese granitic batholith of the Lhasa Terrane and the Luobusha Formation, which is a Tertiary Oligo–Miocene molasse deposit (Huang et al., 2014).

Studies on the entire Yarlung Zangbo ophiolite proposed that the mantle peridotites outcropped in the Yarlung Zangbo ophiolite belt are probably subcontinental lithospheric mantle beneath the Asian plate (Wu et al., 2014). During the Early Cretaceous, extension of the leading edge of the Asian continent resulted in the exhumation of the subcontinental lithospheric mantle and the formation of an oceanic basin. Exhumation and thinning of the lithosphere resulted in upwelling and melting of the asthenosphere, which led to the eruption of basalt and intrusion of gabbro and dolerite. During the maximum extension, partial melting of the metasomatized refractory lithosphere mantle gave rise to some amount of boninitic melts. Yarlung Zangbo ophiolite is much different from the ideal ophiolite section defined by the Penrose Conference, and it could not be considered a remnant of the Neo-Tethyan Ocean between the Indian and Asian continents. Yarlung Zangbo ophiolite represents an oceanic lithosphere formed at an ultraslow spreading center with a spreading rate much lower than that in Western Alps (Wu et al., 2014).

3 Materials and methods

Thin sections were examined using a polarizing microscope and by scanning electron microscopy. Optical analyses were performed using a standard polarized light microscope (Leica DM2700P). Backscattered electron (BSE, atomic Z-contrast) analyses were carried out using an FEI Nova NanoSEM 450 equipped with a Nordlys Nano detector at the Institute of Geology and Geophysics, Chinese Academy of Sciences (IGGCAS), Beijing. Mineral chemistry analysis was performed using a wavelength-dispersive (WDS)

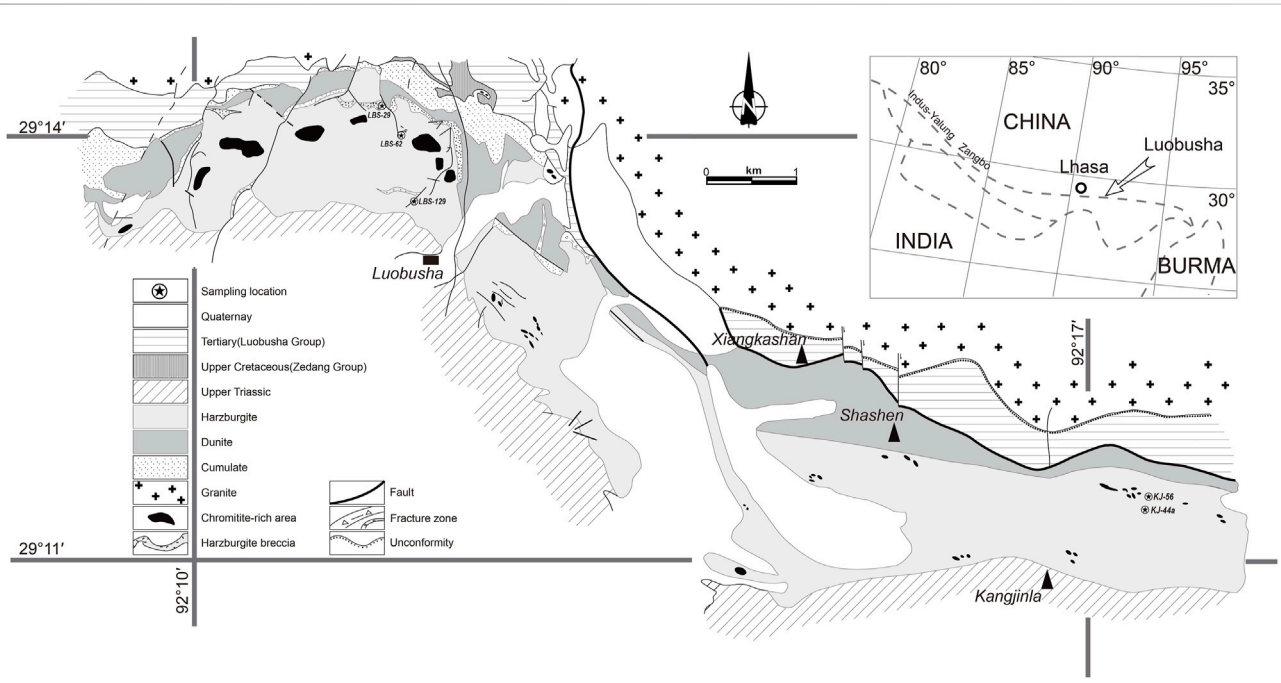

FIGURE 1
Geological map of the Luobusha ophiolite, Tibet, SW China [simplified from the work of Zhang et al. (1996)].

TABLE 1 Mineral composition of zoned olivine and the matrix from the pseudotachylyte veins. Listed cations follow the formula with Fe^{3+} corrected according to the work of Droop (1987), Mineralogical Magazine, v. 51, pp. 431–435. Total*s: Recalculated on an anhydrous basis to a total of 100%. Mineral abbreviations are according to the work of Whitney and Evans, 2010, with ol referring to olivine.

PST zoned olivine core						PST zoned olivine rim					PST matrix							
Sample	KJ-44a	KJ-44a	KJ-56	KJ-56	LBS-29	KJ-44a	KJ-44a	KJ-56	KJ-56	LBS-29		KJ-44a	KJ-44a	KJ-56	KJ-56	LBS129	LBS-62	12LBS29
SiO_2	41.19	41.11	41.09	40.94	40.91	40.10	40.96	40.27	40.23	41.04	SiO_2	40.98	41.11	42.55	41.87	38.94	39.92	41.19
TiO_2	0.00	0.00	0.02	0.00	0.03	0.01	0.00	0.01	0.02	0.00	TiO_2	0.01	0.02	0.00	0.00	0.02	0.04	0.02
Al_2O_3	0.06	0.02	0.03	0.00	0.00	0.07	0.10	0.07	0.44	0.30	Al_2O_3	0.02	0.07	0.09	0.21	0.16	0.10	0.00
Cr_2O_3	0.05	0.05	0.03	0.02	0.03	0.08	0.06	0.14	0.24	0.22	Cr_2O_3	0.00	0.01	0.00	0.01	0.10	0.08	0.04
FeO	8.27	8.50	8.53	8.93	9.34	11.50	11.28	12.89	11.69	12.68	FeO	5.30	4.41	3.82	3.62	6.76	5.94	4.86
MnO	0.11	0.11	0.10	0.13	0.16	0.19	0.24	0.22	0.25	0.19	MnO	0.10	0.06	0.07	0.02	0.16	0.10	0.08
NiO	0.39	0.38	0.38	0.34	0.37	0.36	0.35	0.36	0.36	0.31	NiO	0.07	0.07	0.22	0.10	0.16	0.13	0.05
MgO	50.04	51.00	49.75	49.89	49.24	47.82	47.47	46.55	45.74	46.39	MgO	40.52	39.08	39.89	39.58	40.44	42.62	39.76
CaO	0.04	0.00	0.04	0.01	0.03	0.02	0.02	0.03	0.05	0.05	CaO	0.02	0.02	0.03	0.04	0.14	0.08	0.03
Total	100.16	101.18	99.98	100.30	100.16	100.17	100.50	100.57	99.03	101.19	Total	87.05	84.90	86.69	85.49	87.05	89.05	86.05
O = 4											H_2O	12.59	12.37	12.69	12.53	12.39	12.75	12.49
											Total*	99.61	97.22	99.35	97.97	99.27	101.74	98.51
											O = 7							
Si	1.00	0.99	1.00	1.00	1.00	0.99	1.01	1.00	1.01	1.01	Si	1.93	1.99	2.02	2.01	1.84	1.83	1.97
Ti	0.00	0.00	0.00	0.00	0.00	0.00	0.00	0.00	0.00	0.00	Ti	0.00	0.00	0.00	0.00	0.00	0.00	0.00
Al	0.00	0.00	0.00	0.00	0.00	0.00	0.00	0.00	0.01	0.01	Al	0.00	0.00	0.01	0.01	0.01	0.01	0.00
Cr	0.00	0.00	0.00	0.00	0.00	0.00	0.00	0.00	0.00	0.00	Cr	0.00	0.00	0.00	0.00	0.00	0.00	0.00
Fe^{3+}	0.00	0.02	0.00	0.01	0.00	0.02	0.00	0.00	0.00	0.00	Fe^{3+}	0.13	0.01	0.00	0.00	0.27	0.23	0.06
Fe^{2+}	0.17	0.15	0.17	0.18	0.19	0.22	0.23	0.27	0.25	0.26	Fe^{2+}	0.08	0.17	0.15	0.14	0.00	0.00	0.13
Mn	0.00	0.00	0.00	0.00	0.00	0.00	0.00	0.00	0.01	0.00	Mn	0.00	0.00	0.00	0.00	0.01	0.00	0.00
Ni	0.01	0.01	0.01	0.01	0.01	0.01	0.01	0.01	0.01	0.01	Ni	0.00	0.00	0.01	0.00	0.01	0.00	0.00
Mg	1.82	1.83	1.81	1.81	1.80	1.76	1.74	1.72	1.71	1.70	Mg	2.85	2.82	2.82	2.83	2.85	2.92	2.83
Ca	0.00	0.00	0.00	0.00	0.00	0.00	0.00	0.00	0.00	0.00	Ca	0.00	0.00	0.00	0.00	0.01	0.00	0.00
Total	3.00	3.00	3.00	3.00	3.00	3.00	3.00	3.00	3.00	3.00	Total	5.00	5.00	5.00	5.00	5.00	5.00	5.00
											OH	4.00	4.00	4.00	4.00	4.00	4.00	4.00
X_{Mg}	0.91	0.92	0.91	0.91	0.90	0.89	0.88	0.86	0.87	0.87		0.97	0.94	0.95	0.95	1.00	1.00	0.95

10.3389/feart.2023.1267211

electron microprobe analyzer (JEOL JXA-8100) at IGGCAS. Well-characterized natural samples were used as standards. The operating conditions for the analyses are as follows: the accelerating voltage was 15 kV for silicates and 20 kV for sulfides; beam current was 10 or 20 nA for silicates and 20 nA for sulfides; focus beam diameter was 3 μm for matrix and big inclusions but 1–2 μm for tiny inclusions; and counting time was 20 s for Na, Mg, Al, Si, Ca, and Fe, 30 s for Cr, and 10 s for K, Mn, Ti, Ni, F, Cl, and S. The JEOL ZAF program was used for matrix correction. Light elements (F, Cl, and Na) were analyzed first during the analytical sequence to minimize the effect of migration. Representative analyses are presented in Figures 5, 6; Table 1.

4 Petrography

Our samples of pseudotachylytes derived from harzburgite were collected at the ore districts of Luobusha and Kangjinla, which, together with the Xiangkashan ore district, are commonly called Luobusha. In outcrop, it is not easy to distinguish between pseudotachylyte veins and the commonly present serpentine veins, which became a huge disadvantage for our recognition. Further identifications were carried out through detailed petrographic observations on a thin-section scale and analysis in the laboratory.

In most cases, the ultramafic pseudotachylytes found in Luobusha formed simple veins and complex networks (Figures 2A–D) within micro-damage zones. The thin-section examination showed that the micro-damage zones containing hairline-thin ultramafic pseudotachylyte veins formed in the harzburgites were less than 2 mm wide in general. A characteristic feature of individual damage zones containing pseudotachylyte veins was that they form an asymmetrical network composed of highly fractured and net-veined host rock fragments. Simple pseudotachylyte veins occurred as the core of the micro-damage zones (Figures 2A–D) and varied in thickness of a small range from ca. 50 μm to an observed width of 200 μm in thin sections. Transmitted light microscopy revealed that the simple pseudotachylyte veins, which occasionally branched off on the local scope, are darker than the host rock fragments. Some opaque mineral assemblages occurred as contact with the dominant transparent minerals with different levels of granularity. These opaque minerals were magnetite and, in general, cemented with serpentine that came into being on account of the hydration of the olivine fragments at a later stage. So, the serpentine takes on banded occurrence stretching parallel to the micro-damage zones (Figures 2A, B, D). Flow structures (Figure 2C) were seen in places, indicating the presence of flow along the fracture. The pseudotachylytes were also associated with cataclasite and ultra-cataclasite veins consisting of ultrafine-grained pulverized lithic fragments and clasts, which make them seem like an “ultrafine fracture zone” across the entire thin section under the optical microscope (Figures 2G, H). The high-magnification microscopic observation roughly revealed that the pseudotachylyte veins are composed of close-knit ultrafine-grained minerals, but their boundary could not be discerned even with the aid of the highest microscopic power (Figure 2D). In view of the petrographic feature described above, in our pilot case study of the pseudotachylyte veins from Luobusha, only via optical microscopy, we recognized these veins just as micro-damage zones or ultra-cataclasites before we were fully convinced that these veins were ultrafine pseudotachylyte by scanning electron microscopy.

For these micro-pseudotachylyte veins, polarizing microscopy can only reveal their rough geometric and morphological features. When we used the eyepiece of ×10 combined with the objective of ×50, the morphology and size of the ultrafine minerals in the pseudotachylyte veins were hardly discerned because the view area was fairly fuzzy and gloomy. As a result, we could not make out the detailed structures of these veins by polarizing microscopy, let alone discover the types of minerals in the veins. Further works have been carried out by scanning electron microscopy and electron microprobe analyses. High-resolution scanning electron microscopy examination and analyses of chemical compositions show that the ultrafine granules in the pseudotachylyte veins are mainly olivine, orthopyroxene, serpentine, spinel, and magnetite. These fine-grained minerals are less than 10 μm, and very few are more than 50 μm, generally cemented by an extremely fine interstitial material. Olivine is the primary component of the pseudotachylyte veins occurring as microphenocrysts, showing zoning from core to rim and as extremely irregular-shaped microlite immersed in the interstitial material (Figures 3A–D). They are less variable in grain size (<10–20 μm). The olivine microphenocrysts in the pseudotachylyte veins are distinctly zoned with darker cores and bright rims, and some grain boundaries are jagged, indicating obvious geochemical zoning (Figures 3B–D). The olivine microlites (<1 μm) are granular and vermicular in shape. In some samples, the olivine microlites within the pseudotachylyte vein are extremely irregular, which can be referred to as dendritic and skeletal crystals (Figures 4A–D). Most of the crystal boundaries are serrated and flame-like. Tabular and fibrous microcrystals developed as interstitial material in the space between poikilitic olivine grains (Figure 4A). The interstitial matrix between microphenocrysts and microlites has a lower average atomic weight and low total oxide analyses (<90%), exhibiting micro-fibers and micro-pores in the BSE images obtained under a high magnification of field emission high-resolution scanning electron microscopy, and the black domains represent micro-cavities in the interstitial matrix between the new-formed crystallites (Figure 3H and Figures 4E, F). Minor orthopyroxene porphyroclasts were cemented by the fine-grained variable amounts of olivine crystallites. Small irregularly shaped chrome-spinel can be spotted among the interstitial matrix. These chrome-spinel crystals are snowflake- or coral-like in form and have a higher average atomic number (bright) along the rims, indicating chemical zonation (Figures 3B, E, G). They are less than 10 μm across and may represent Fe-rich rim overgrowth. In addition, the interstitial matrix contains nanoparticles of Ni sulfide grains. These Ni sulfide grains identified via electron probe microanalysis are often ~1–2 μm across and intersperse among the matrix like a droplet (fine bright spots) and may imply melt occurrence (Figures 4A, C). The pseudotachylyte veins are marked by streaks and bands, indicating compositional variation and textural zoning (Figures 2B, D). BSE (backscattered electron) imaging shows that these pseudotachylyte veins feature the average atomic contrast (zones of different brightness) (Figures 2E, F, 3A). The distribution character of the olivine grains in the bright parts is

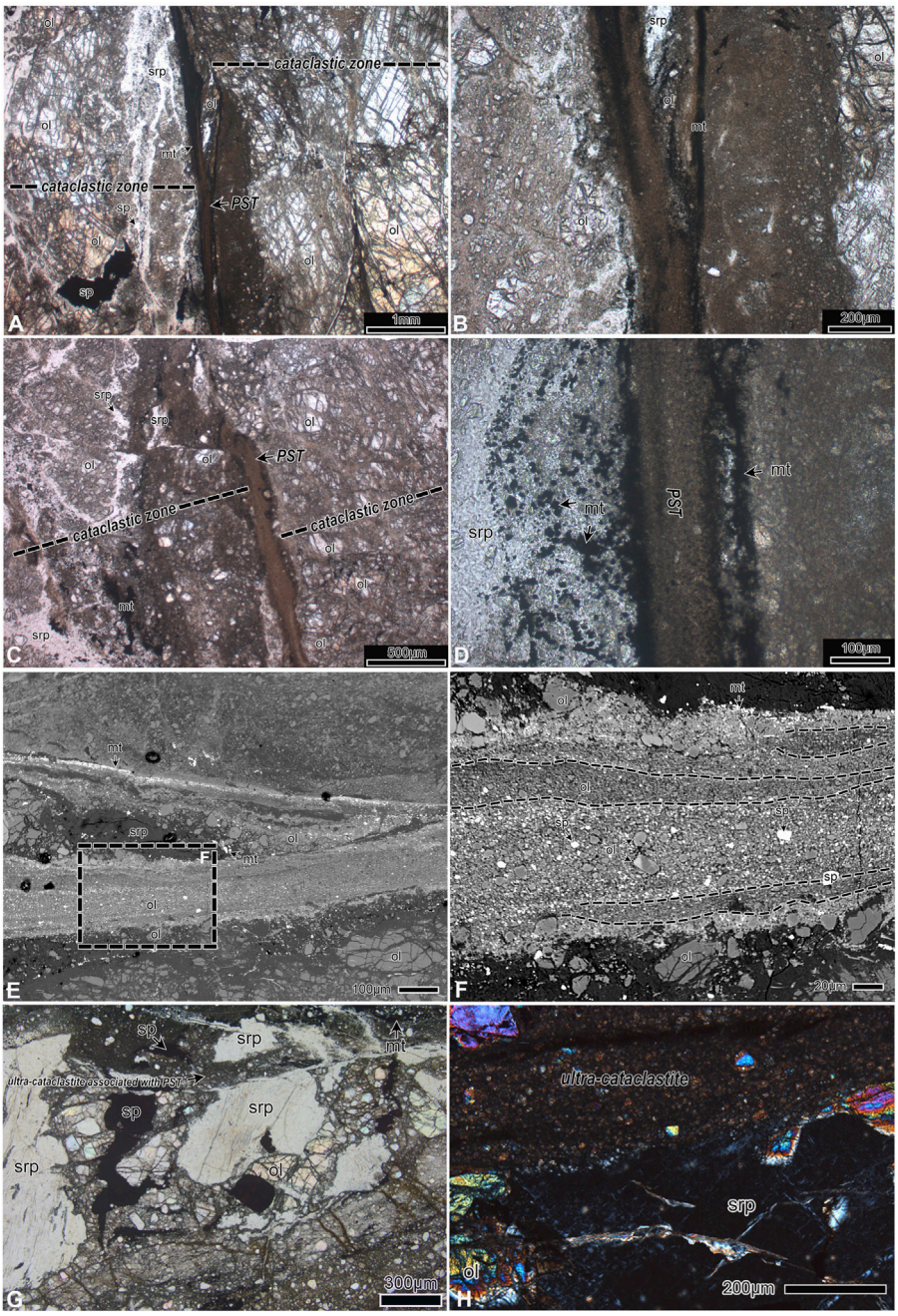

FIGURE 2
Optical and backscattered electron images of pseudotachylyte veins in harzburgites. **(A, B)** Opitcal photomicrograph (plane-polarized light). Hairline-thin pseudotachylyte vein occurred at the central part of the micro-damage zone that is less than 2 mm (max 1.8 mm) wide. The vein can be traced almost continuously across the entire thin section. It should be noted that the vein branched off but did not change the extending direction. The wall rock surfaces are rough with a fractured appearance. The serpentites of the later stage take on banded occurrence stretching parallel to the micro-damage zones. **(C)** Flow banding pseudotachylyte veins occurred within the micro-damage zone. The vein is also hairline-thin and looks like a rivulet making a bend locally under plane-polarized light. **(D)** Microscope examination (plane-polarized light) at high power shows that the pseudotachylyte veins are composed of close-knit ultrafine-grained minerals, but their boundary could not be discerned. Plenty of pulverized minerals are located on both sides of the pseudotachylyte vein. Some opaque mineral assemblages (magnetite) occur as contacts of the dominant transparent minerals with different levels of granularity and are, in general, cemented with serpentites, which were formed by later hydration of the olivine fragments. **(E)** BSE photographs show that pseudotachylyte veins feature the average atomic contrast (zones of different brightness) representing the streaks spotted under the optical scope. **(F)** Framed detail in (E) displays compositional variation and textural zoning of pseudotachylyte veins. **(G, H)** Optical photomicrographs showing that ultracataclastite associated with pseudotachylyte veins and ultracataclastite transecting serpentine porphyroclast under plane-polarized light and cross-polarized light, respectively. Mineral abbreviations are according to the work of Whitney and Evans (2010), with ol referring to olivine, srp to serpentite, mt to magnetite, sp to spinel, and cmt to chromite.

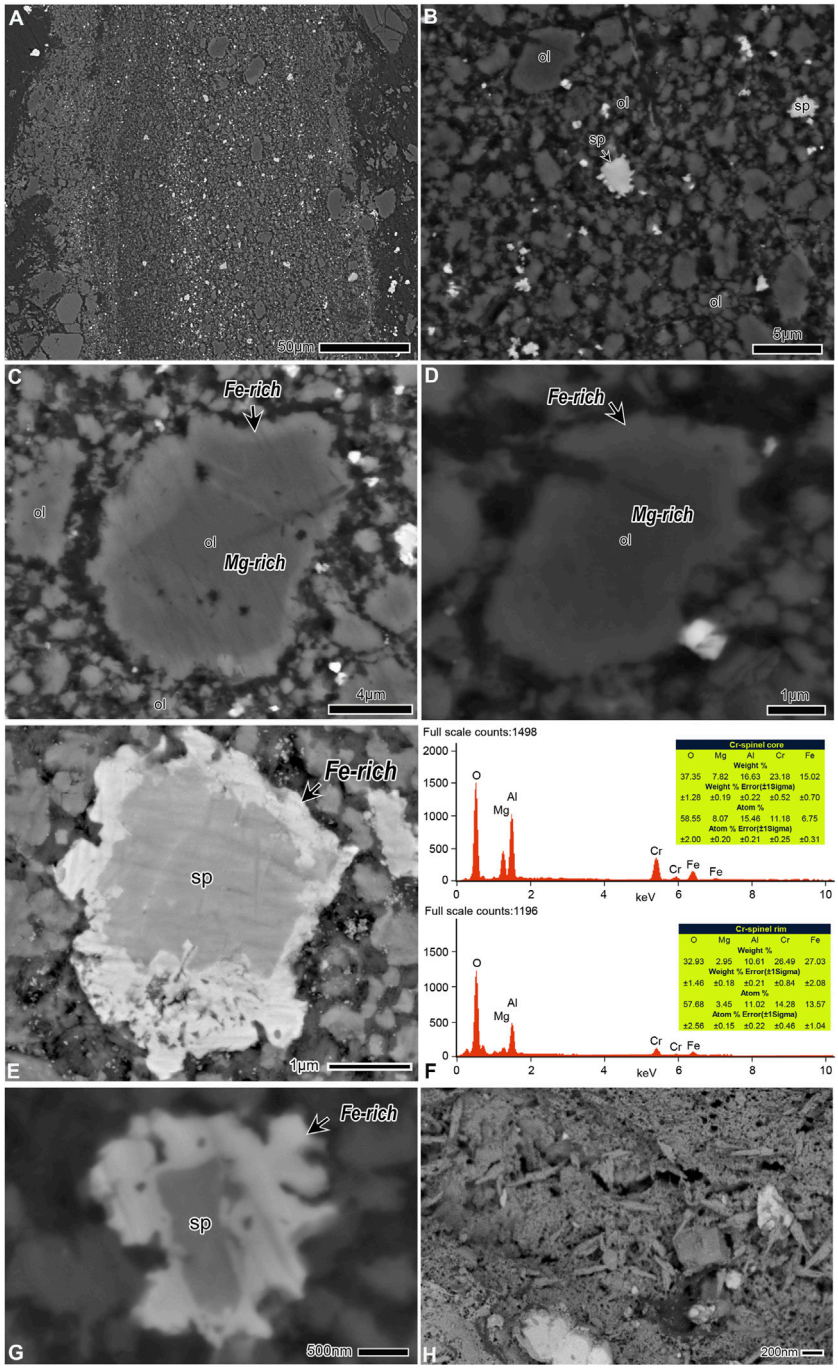

FIGURE 3
Back-scattered electron images obtained using field emission electron microscopy. **(A)** The average atomic contrast is evident. The darker part is attributed to a cluster of densely packed olivine microlites and interstitial material. Spinel and magnetite particles arranged along the extension direction of the pseudotachylyte vein forming a narrow bright stripe. **(B)** Sub-idiomorphic olivine microphenocrysts and vermicular olivine microlites are cemented by interstitial material. **(C, D)** Zoning texture of olivine grains. The darker core is relatively rich in Mg, whereas the bright rim is relatively rich in Fe. It should be noted that the grain boundaries are uneven and serrated. **(E, G)** Chemically zoned chrome-spinel with an Fe-rich rim overgrowth. **(F)** Energy-dispersive spectrometry result reveals that the rim of the chrome-spinel in **(E)** is rich in Fe compared to the core. **(H)** The micro-cavities are visible in the micro-fibrous and micro-porous interstitial material.

that the microphenocrysts are surrounded by densely packed irregularly shaped crystals. These crystals are very tiny, generally not more than 5 microns, which are recognized as olivine microlites. However, some of the microphenocrysts are more than 10 microns across. The matrix in the gap between the particles is composed of serpentine minerals (Figures 2F, 3A). The darker part of these pseudotachylytes consists of worm-like olivine microlites densely interconnected with each other. The interspace matrix also features a lower average atomic weight (Figures 3A, B). Ultracataclastite and ultracataclastite associated with pseudotachylyte veins transected serpentine (Figures 2G, H). Within the

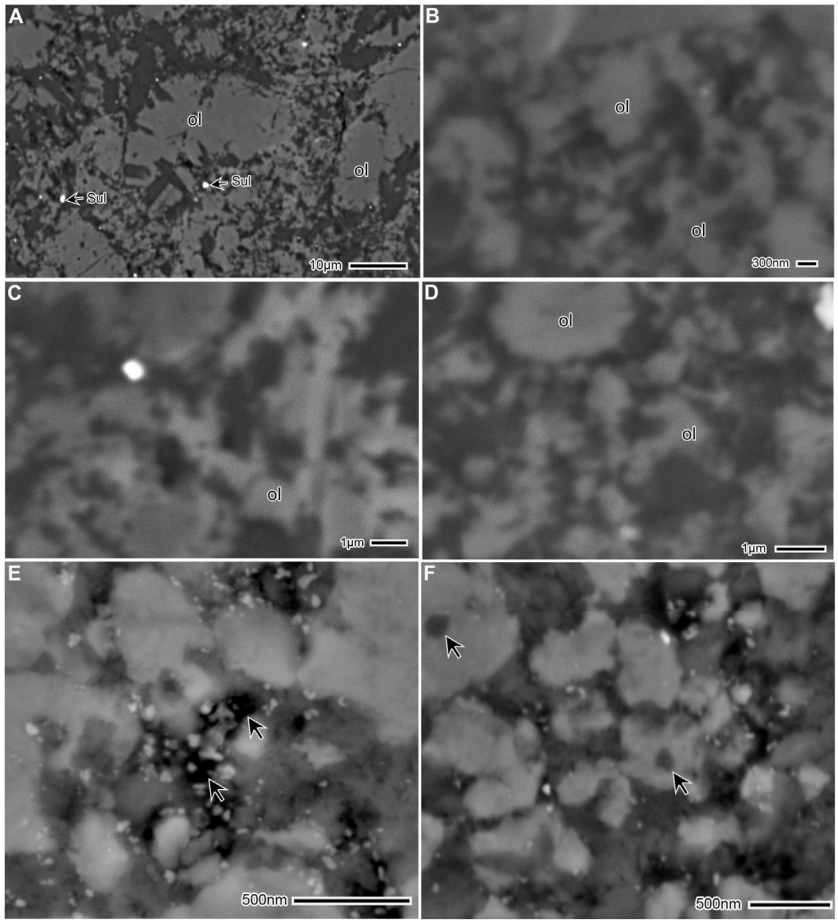

FIGURE 4
Back-scattered electron images showing the microtexture of microlites of olivine and the interstitial matrix. **(A)** Poikilitic and skeletal olivine microlites and interstitial matrix. Most of the crystal boundaries are serrated and flame-like. The Ni sulfide (Sul) granules should also be noticed. **(B–D)** High-resolution scanning electron microscopy photographs of micro-dendritic and skeletal microlites of olivine and the interstitial matrix. **(E, F)** The olivine microlites are cemented by flocculent and spongiform interstitial materials. Extremely tiny globular inclusions (arrowed) in the core of the olivine microlites are shown. They have a lower average atomic weight compared to host olivine microlites and are speculated to be prograde serpentine inclusions. The arrows in **(E)** indicate miniscule micro-cavities.

pseudotachylyte, it is visible that some punctiform inclusions developed in the olivine microlites and might be serpentine presumably (Figures 4E, F).

5 Mineral chemistry

The comparative study of chemical composition between pseudotachylyte veins and host rock is a common analytical method used by researchers. Representative analyses are presented in Figures 5, 6; Table 1. Mineral formulae were calculated by assuming stoichiometry and charge balance (Droop, 1987). Electron microprobe (EMP) analyses show that the olivine in the host harzburgite is homogeneous (Fo_{90-92}) (Figure 5), whereas olivine microphenocrysts in the pseudotachylyte are quite heterogeneous, ranging from Fo_{85}–Fo_{92}, and display chemical zonation characteristics with Mg-rich cores (Fo_{90-92}) and higher Fe-content along the margins (Fo_{86-89}) (Table 1). The forsterite contents of the microlites fall in between the former two occurrences of olivine in the diagrams (Figure 5), ranging from Fo_{87}–Fo_{92}. The significant feature of the olivine microlites is that they contain significant amounts of Ca, Al, and Cr compared with the olivine in the host harzburgite recognized from the diagrams (Figures 5, 6). However, it is noted that olivine microlites and the microphenocrysts in pseudotachylyte have a lower Ni content compared to the host harzburgite olivine (Figures 5, 6).

The pseudotachylyte micro-fibrous and micro-porous interstitial matrix between microphenocrysts and microlites contains a large number of extremely fine materials below the spatial resolution of our instrumentation, which makes it difficult to accurately determine the chemical composition. BSE images show that the interstitial matrix has a low average atomic weight. EMP analyses give a range of ultramafic compositions with SiO_2 and MgO contents from 38.9%–42.5% and 39.0%–42.62%, respectively. The analyses give low totals ranging from 84.9%–89.05% and total*s 97.2%–101.74% recalculated on an anhydrous basis to a total of 100% (see Table 1). It can be interpreted that the analyses represent mixed data and do not reconcile with real mineral compositional variations.

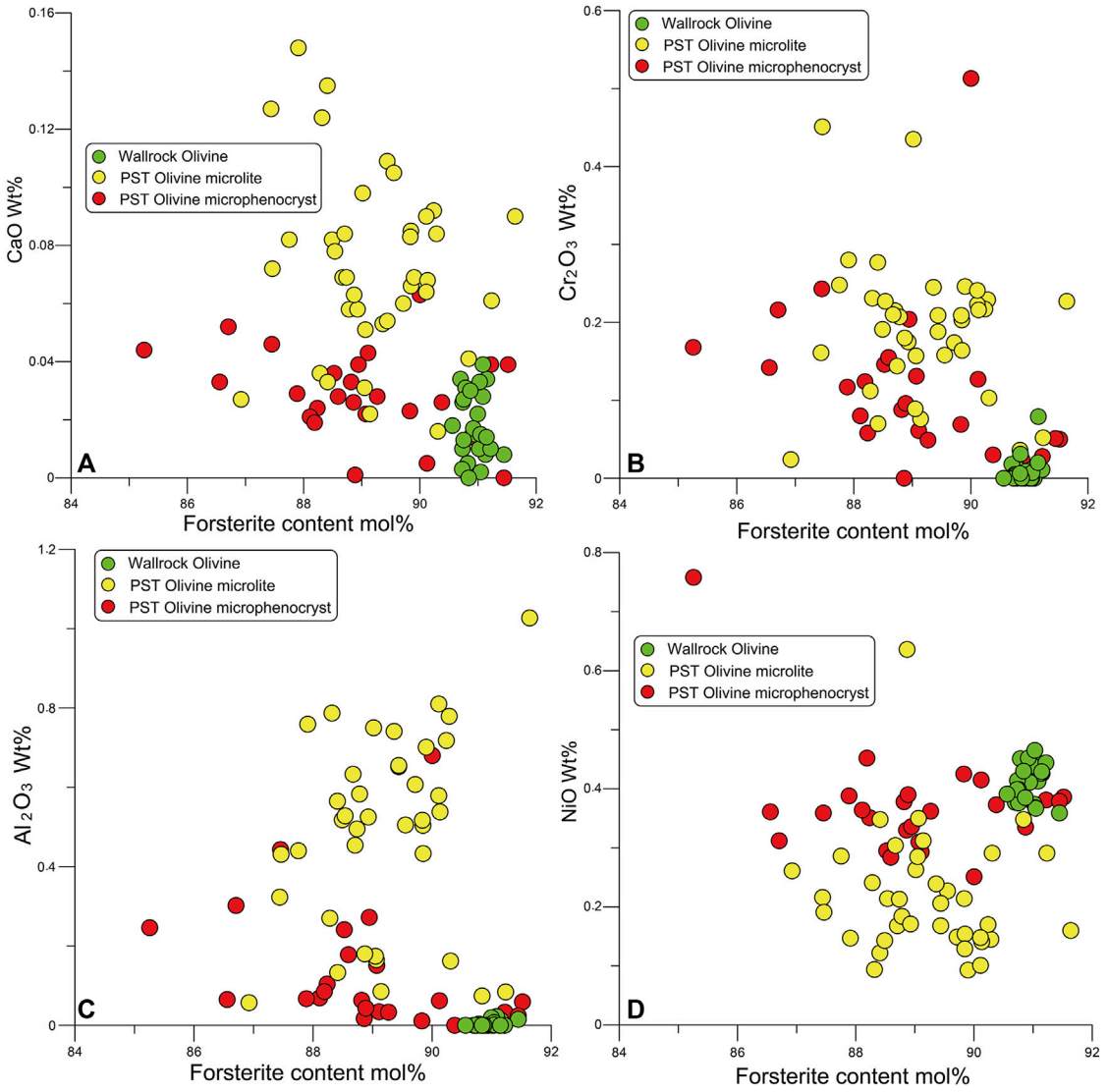

FIGURE 5
Ca **(A)**, Cr **(B)**, Al **(C)**, and Ni **(D)** contents versus the Fo content of olivine in three main occurrences from the pseudotachylyte veins obtained by electron microprobe analysis.

In addition, the rims of zoned irregularly shaped chrome-spinel are higher in Fe (27.03 wt%) and lower in Mg (2.95 wt%) than their cores that contain lower Fe (15.02 wt%) but higher Mg (7.82 wt%) obtained by using an energy-dispersive spectrometer (EDS) equipped on the scanning electron microscope (Figure 3F). Despite a semi-quantitative analysis, the Mg–Fe zoning from core to rim has been well revealed.

6 Discussion

6.1 Type of injection vein

Most of the sampled veinlets with dark-brown color, dense and aphanitic appearance, and occurrence as both simple veins and irregular networks are typically very thin (~2 cm), similar to the ultramafic pseudotachylyte from a spinel lherzolite mass in the Ivrea–Verbano zone, Northern Italy (Obata and Karato, 1995). Most pseudotachylyte veins in mantle peridotite from the Alpine subduction complex of Corsica are less than 2 cm thick (Andersen and Austrheim, 2006). The pseudotachylyte veins from the Luobusha peridotite complex are so hairline-thin that they can only be identified in thin sections and can hardly be discerned in outcrop. Very thin injection veins require extremely low viscosity for the melt. High-pressure experiments showed that ultramafic melts have very low viscosities of 10^{-1} Pa·s or less (Suzuki et al., 2001). Such low viscosity is consistent with the intrusive features associated with the mm-thin ultramafic pseudotachylytes. The mm-to-cm-thin veins must have been emplaced and solidified in seconds and ca 10–15 min, respectively (Andersen and Austrheim, 2006). The experimentally generated injection veins of ultramafic pseudotachylyte that formed during the serpentinite high-velocity friction experiments ranged in width from 0.1 to 0.5 mm (Lin et al., 2013). Based on vein geometry, the individual veins and network veins within Luobusha peridotite are

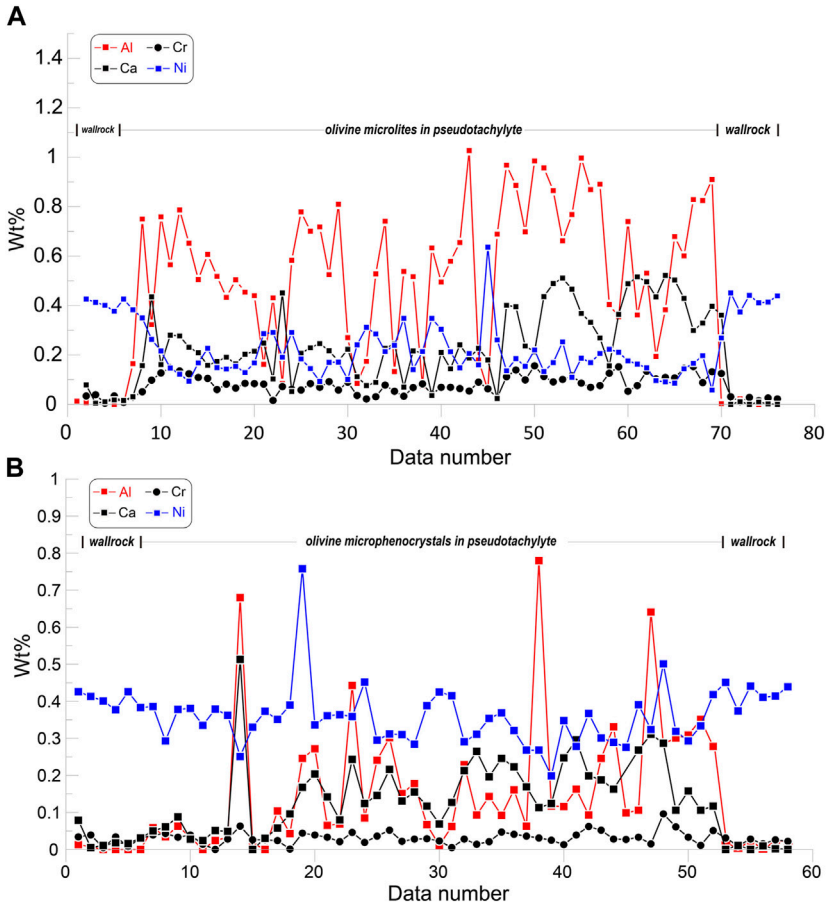

FIGURE 6
Compositional profiles of olivine microlites **(A)**, microphenocrysts **(B)**, and wall rock olivine within a transect spanning the pseudotachylyte and wall rock on each side.

injection veins. The fragment-bearing frictional melt moves rapidly from the generation zone to the void spaces within dilational fractures that formed at the same time as the pseudotachylyte. Rapid injection under thermal pressurization of the melt associated with expansion is related to frictional heating within the pseudotachylyte generation zone and syn-dilational fractures formed by seismic rupture (Lin, 2008). Dilational fractures often contain a zone of cataclasite (Lin, 2008), which can account for the occurrence that pseudotachylyte veins are bound by micro-damage zones.

6.2 Diagnostic quenching microtextures and chemical inhomogeneties

The microlites in the pseudotachylyte veins are extraordinarily fine-grained, showing certain melting and recrystallization characteristics. In particular, some olivine microphenocrysts display characteristic textures of minerals crystallized from the melt and chemical zonation generated at high temperatures. The olivine crystals are zoned with Mg-rich cores and more Fe-rich margins. This zoning pattern is typical evidence of crystallization from friction melts (Obata and Karato, 1995; Andersen and Austrheim, 2006). The preservation of Fe–Mg zoning at the scale of ~1 μm indicates that the cooling time was shorter than 10^2 s, which suggests that the formation of the pseudotachylyte was associated with co-seismic faulting (Buening and Buseck, 1973; Obata and Karato, 1995). In addition, snowflake- and coral-like chrome-spinel are chemically zoned as well. The spinel crystals have Mg–Fe zoning from core to rim, indicating Fe-rich rim overgrowth, which are similar to those described by Andersen in Corsica ultrabasic pseudotachylyte veins (Andersen and Austrheim, 2006). The compositional variations between the wall rock and the pseudotachylyte minerals are blindingly obvious. Olivine in the host harzburgite is more restricted ($Fo_{90–92}$), whereas the microphenocrysts in the pseudotachylytes are very heterogeneous, ranging from Fo_{85}–Fo_{92}. The forsterite contents of the microlites fall in between the former two occurrences of olivine in the diagrams (Figure 5), ranging from Fo_{87}–Fo_{92}. The microphenocrysts, especially some microlites in the pseudotachylyte, have higher CaO contents than the host harzburgite olivine and also have higher Cr_2O_3 and Al_2O_3 (Figures 5, 6). The high Cr content of the olivine microcrystals supports the hypothesis of a high-temperature origin for the pseudotachylyte. High abundances of Ca and Cr in olivine are often observed for rapidly grown crystals from high-temperature ultramafic magmas, such as komatiites (Arndt et al., 1977; Obata and Karato, 1995). Olivine crystals can

accommodate significant amounts of Cr^{2+} at high temperatures, even at typical terrestrial oxidation conditions, and the solubility of Cr^{2+} increases effectively with an increase in temperature (Li et al., 1995; Obata and Karato, 1995). The high Ca and Cr contents of olivine microphenocrysts support the view that their zoning pattern is consistent with interpreting that the olivine is precipitated as crystal from the melt. However, it is noted that the olivine microlites and the microphenocrysts in pseudotachylyte have a lower Ni content compared to the host harzburgite olivine. Some nanoparticles of Ni sulfide droplets have been observed in the interstitial matrix, which is akin to the previously described examples of pseudotachylyte from the Balmuccia peridotite (Ueda et al., 2008) and the Alpine Corsica complex (Andersen and Austrheim, 2006). Both of them were interpreted to crystallize directly from the frictional melt. The loss of Ni in the olivine during the melting process results in the formation of sulfide in the newly crystallized pseudotachylyte matrix, which may account for observed lower Ni contents in the newly formed microcrystalline olivine. As a consequence, we interpret the high Ca and Cr contents and lower Ni contents of olivine grains to be crystallized directly from the friction melt. The chemical inhomogeneties, that is to say, the zoning patterns as well as the compositional variations between the host harzburgite and the pseudotachylyte minerals, are very similar to those of the pseudotachylyte from the Balmuccia peridotite and the Alpine Corsica complex (Obata and Karato, 1995; Andersen and Austrheim, 2006).

The interstitial matrix between microphenocrysts and microlites appears micro-fibrous and micro-porous. The micro-cavities are visible when observed by field emission high-resolution scanning electron microscopy (SEM) in the interstitial matrix between the newly formed crystallites. SEM examination shows that the interstitial matrix between microphenocrysts and microlites has a lower average atomic weight and low total oxide analyses (<90%) exhibiting fibrous and cotton-like in the BSE image obtained under high magnification of SEM, and the black domains represent cavities (Figures 3H, 4E, F). These cavities probably represent vesicles present at the melt stage since olivine crystals have crystallized into the cavities. The presence of a micro-vesicular interstitial matrix suggests that the frictional melting was accompanied by high fluid pressures, which, at least locally, was sufficient to release a free gas phase from the melt. The fibrous domains of the matrix were probably formed via the devitrification of the original glass to serpentine (Andersen and Austrheim, 2006).

6.3 Rate of deformation and co-seismic transient high-pressure metamorphism (dehydration) in the crust

Rock textures and microstructures can be used to infer the rate of deformation and associated high-pressure metamorphism. For instance, quench textures formed by spherulites, dendrites, and skeletal, acicular, or poikilitic microlites can be recognized in rocks crystallized from volcanic and friction or shock melts (Sibson, 1975; Lin, 2008; Yang et al., 2016). The dendritic textures are formed by rapid cooling only under limited conditions where the growth rate of crystals is fast in comparison to the nucleation rate (Chalmers, 1964). The crystallization of microlites from friction melt would imply that the duration of the high-pressure metamorphism was very brief owing to the co-seismic nature of the melt (Yang et al., 2016). Furthermore, porphyroclasts dominated by thermally rounded olivine and minor orthopyroxene can be observed. The disequilibrium feature of the clasts suggests that there exists very rapid heating (Swanson, 1992).

It is observed that ultracataclastite veins are associated with pseudotachylyte transecting serpentine. In the sampled pseudotachylytes, some extremely tiny globular inclusions (~100 nm) can be observed in the core of the olivine microlites under a high-resolution scanning electron microscope. These inclusions have a lower average atomic weight compared to host olivine microlites (Figures 4E, F). As they are extremely minuscule with a nanometer scale of particle size, existing analytical methods are not suitable for mineral identification and chemical composition analysis. Based on the lower average atomic number, these tiny inclusions would be prograde serpentine. For complete reaction, serpentine disappears before olivine is crystallized during prograde metamorphism, simulated by P-T pseudosection for the harzburgite in the system $CaO–FeO–MgO–SiO_2–H_2O$ (Huang et al., 2014). Reaction kinetics has played a role in the preservation of portions of the serpentinite minerals in the peridotite minerals. The preservation of serpentine (lizardite) as inclusions in the high-pressure minerals implies that the breakdown of lizardite was slower than the P-T increase such that olivine started to grow while a portion of lizardite persisted (Huang et al., 2014), which means that the high-pressure metamorphism took place rapidly. Frictional heating in ultracataclastite associated with pseudotachylyte veins would dehydrate hydrous minerals (serpentine) to their corresponding products (olivine) of high-pressure metamorphism. This characteristic and attractive feature was also observed in pseudotachylyte-like veins from Corsica, where serpentine inclusions were partly surrounded by neoblastic olivine (Austrheim and Andersen, 2004).

A question arises then as to how a prograde serpentine could be enclosed in the olivine microlites quenching from the melt. High-velocity friction experiments on serpentinite under conditions equivalent to large amounts of earthquake slip show that both serpentine and olivine minerals were melted by friction heating. Rapid serpentine dehydration occurred in a zone of up to ~3 mm wide. Dehydration reactions of serpentine can be caused by frictional heating that accompanies frictional melting in the slip zone and its bounding zones (Lin et al., 2013). The microtexture shown in Figure 4F implies a partial melting and multiple stages of co-seismic friction. The serpentine minerals were melted during the formation of the former pseudotachylyte and then quenched into microlites of serpentine. Further frictional heating overprinting pre-existing pseudotachylyte resulted in the breakdown (dehydration) of serpentine into high-pressure microlites of olivine.

The wall rock to the pseudotachylyte and associated ultracataclastite was subjected to serpentinization after having emplaced in the crust and then transformed back into peridotite by subsequent high-pressure metamorphism at Luobusha (Huang et al., 2014). The pseudotachylytes were generated in the crust after the high-pressure metamorphism and did not recede to a greater depth. If the rocks were held at great depths after the seismic events, then the quenching textures would have been erased due to

continuous mineral growth. So, we hold the opinion that flash ultra-comminution and frictional heating may release fluids by localized heat-driven prograde reactions in the crust, which appears to be the more likely process for the preservation of the petrographic features in the present study.

6.4 Physical origin of pseudotachylyte in Luobusha peridotite

Clarification of the physical origin of pseudotachylyte is complicated by its very fine-grained nature, the common presence of devitrified and recrystallized material and rock fragments, and the obscuring effects of subsequent deformation, alteration, and metamorphism (Lin, 2008). It is clear that glass or glassy material within pseudotachylyte indicates the generation of melt during its formation, but the converse is not true: the absence of glass or glassy material is not a diagnostic test for the melting origin for pseudotachylyte because primary glass or glassy material can be devitrified during subsequent alteration and/or metamorphism (Lin, 2008). In addition to the melting-origin pseudotachylyte, crushing-origin pseudotachylytes, which are generated by rapid comminution and injection during seismic faulting, are also considered to represent fossil earthquakes, as with melt-origin pseudotachylytes (Kano et al., 2004; Lin, 2008). Such veins are mainly composed of fine-grained fragments of the wall rock, with little or no evidence of melting (Lin, 2008). However, there exists a gradation from melting-origin pseudotachylyte, which is mostly composed of glass or glass-derived material, to crushing-origin pseudotachylyte (Lin, 2008). The pseudotachylytes in Luobusha peridotite are often associated with ultracataclastite veinlets and are of injection vein type. The pseudotachylytes occurred as thin layers in the core of micro-damage zones. In the immediate vicinity of the pseudotachylyte veins, it is visible that the olivine, pyroxene, and serpentine display strong brittle deformation, and a large number of network cracks developed in the harzburgite wall rock. The cracks are filled with extremely fine crushed minerals of irregular shape. Banding defined by clusters of microphenocryst, microlites, and interstitial material and variable content of thermally rounded olivine in the pseudotachylytes indicate inefficient mixing of the melt, which implies mixed genesis of a combination of crushing and melting. Flash ultra-comminution was associated with frictional heating. It follows from the description and interpretations stated earlier that strong abrasion and ultra-comminution generated during rapid seismic faulting melted rock within the fault zone and fluidized ultrafine-grained material, ultimately producing pseudotachylyte in the studied peridotite rocks.

7 Conclusion

Large paleo-earthquakes have been frozen in ultramafic pseudotachylyte from the Luobusha ophiolite complex in the Yarlung Zangbo suture zone, evidenced by the petrography and mineral chemistry data presented here. The hairline-thin pseudotachylyte veins were formed by rapid injection along dilational fractures from the generation zone produced by strong abrasion and ultra-comminution revealed by the characteristic microtextures and chemical inhomogeneties. Quenching microtextures of olivine and localized shear heat-driven prograde reaction textures demonstrate that the duration of frictional heating within seismic slip zones and associated dehydration reaction of serpentine to olivine was very brief. The Luobusha peridotite is metamorphogenic, which was subjected to serpentinization after having emplaced in the crust, followed by transformation back into peridotite during subsequent high-pressure metamorphism. The pseudotachylytes were generated in the crust after the high-pressure metamorphism and did not recede to a deeper depth. Flash ultra-comminution associated with frictional heating may release fluids via localized heat-driven prograde reactions in the crust.

Data availability statement

The original contributions presented in the study are included in the article/Supplementary Material; further inquiries can be directed to the corresponding authors.

Author contributions

HZ: conceptualization, data curation, investigation, methodology, software, and writing–original draft. XX: conceptualization, funding acquisition, supervision, and writing–review and editing. SY: investigation, methodology, software, and writing–review and editing.

Funding

The authors declare financial support was received for the research, authorship, and/or publication of this article. This work was financially supported by the National Natural Science Foundation of China (Grant 41941016).

Acknowledgments

The authors are very grateful to Tsering Norbu, Lobsang, Tenzin, Nyima Tashi, and Phuntsok for providing great help with field works and sampling at a high altitude.

Conflict of interest

The authors declare that the research was conducted in the absence of any commercial or financial relationships that could be construed as a potential conflict of interest.

Publisher's note

References

Allégre, C. J., Courtillot, V., Tapponnier, P., Hirn, A., Mattauer, M., Coulon, C., et al. (1984). Structure and evolution of the Himalaya–Tibet orogenic belt. *Nature* 307, 17–22. doi:10.1038/307017a0

Andersen, T. B., Austrheim, H., Deseta, N., Silkoset, P., and Ashwal, L. D. (2014). Large subduction earthquakes along the fossil moho in alpine Corsica. *Geology* 42, 395–398. doi:10.1130/G35345.1

Andersen, T. B., and Austrheim, H. (2006). Fossil earthquakes recorded by pseudotachylytes in mantle peridotite from the Alpine subduction complex of Corsica. *Earth Planet. Sci. Lett.* 242, 58–72. doi:10.1016/j.epsl.2005.11.058

Andersen, T. B., Mair, K., Austrheim, H., Podladchikov, Y. Y., and Vrijmoed, J. C. (2008). Stress release in exhumed intermediate and deep earthquakes determined from ultramafic pseudotachylyte. *Geol* 36, 995. doi:10.1130/G25230A.1

Angiboust, S., Agard, P., Yamato, P., and Raimbourg, H. (2012). Eclogite breccias in a subducted ophiolite: A record of intermediate-depth earthquakes? *Geology* 40, 707–710. doi:10.1130/G32925.1

Arndt, N. T., Naldrett, A. J., and Pyke, D. R. (1977). Komatiitic and iron-rich tholeiitic lavas of munro township, northeast ontario. *J. Petrology* 18, 319–369. doi:10.1093/petrology/18.2.319

Austrheim, H., and Andersen, T. B. (2004). Pseudotachylytes from Corsica: fossil earthquakes from a subduction complex. *Terra nova.* 16, 193–197. doi:10.1111/j.1365-3121.2004.00551.x

Austrheim, H., and Boundy, T. M. (1994). Pseudotachylytes generated during seismic faulting and eclogitization of the deep crust. *Sci. New Ser.* 265, 82–83. doi:10.1126/science.265.5168.82

Austrheim, H., Erambert, M., and Engvik, A. K. (1997). Processing of crust in the root of the caledonian continental collision zone: the role of eclogitization. *Tectonophysics* 273, 129–153. doi:10.1016/S0040-1951(96)00291-0

Austrheim, H. (2013). Fluid and deformation induced metamorphic processes around moho beneath continent collision zones: examples from the exposed root zone of the caledonian mountain belt, w-norway. *Tectonophysics* 609, 620–635. doi:10.1016/j.tecto.2013.08.030

Bucher, K. (2005). Blueschists, eclogites, and decompression assemblages of the zermatt-saas ophiolite: high-pressure metamorphism of subducted tethys lithosphere. *Am. Mineralogist* 90, 821–835. doi:10.2138/am.2005.1718

Buening, D. K., and Buseck, P. R. (1973). Fe-Mg lattice diffusion in olivine. *J. Geophys. Res.* 78, 6852–6862. doi:10.1029/JB078i029p06852

Chalmers, B. (1964). *Principles of solidification*. New York: Robert E. Krieger Pub, 319.

Chen, X.-Z., Xia, B., Li, J.-F., Yu, M., Zhang, L.-F., Huang, Q.-T., et al. (2011). Isotopic characteristics and genesis of mantle peridotite from the Luobusha ophiolite. *Geotect. Metallogenia (in Chinese)* 35, 85–94. doi:10.16539/j.ddgzyckx.2011.01.007

Debret, B., Nicollet, C., Andreani, M., Schwartz, S., and Godard, M. (2013). Three steps of serpentinization in an eclogitized oceanic serpentinization front (lanzo massif - western alps): eclogitized serpentinization front (lanzo). *Journal of Metamorphic Geology* 31, 165–186. doi:10.1111/jmg.12008

Deseta, N., Andersen, T. B., and Ashwal, L. D. (2014). A weakening mechanism for intermediate-depth seismicity? Detailed petrographic and microtextural observations from blueschist facies pseudotachylytes, cape corse, Corsica. *Tectonophysics* 610, 138–149. doi:10.1016/j.tecto.2013.11.007

Droop, G. T. R. (1987). A general equation for estimating Fe $^{3+}$ concentrations in ferromagnesian silicates and oxides from microprobe analyses, using stoichiometric criteria. *Mineral. mag.* 51, 431–435. doi:10.1180/minmag.1987.051.361.10

Evans, B. W., and Cowan, D. S. (2012). A Melt origin for spinifex-textured metaperidotite in the Cerro del Almirez massif, southern Spain. *American Journal of Science* 312, 967–993. doi:10.2475/09.2012.01

Evans, B. W., and Trommsdorff, V. (1978). Petrogenesis of garnet lherzolite, cima di Gagnone, lepontine alps. *Earth and Planetary Science Letters* 40, 333–348. doi:10.1016/0012-821X(78)90158-9

Huang, M.-X., Yang, J.-J., Powell, R., and Mo, X. (2014). High-pressure metamorphism of serpentinized chromitite at Luobusha (southern Tibet). *American Journal of Science* 314, 400–433. doi:10.2475/01.2014.11

Jin, D., Karato, S., and Obata, M. (1998). Mechanisms of shear localization in the continental lithosphere: inference from the deformation microstructures of peridotites from the ivrea zone, northwestern italy. *Journal of Structural Geology* 20, 195–209. doi:10.1016/S0191-8141(97)00059-X

John, T., and Schenk, V. (2006). Interrelations between intermediate-depth earthquakes and fluid flow within subducting oceanic plates: constraints from eclogite facies pseudotachylytes. *Geol* 34, 557. doi:10.1130/G22411.1

Kano, K., Lin, A., Fukui, A., and Tanaka, H. (2004). Pseudotachylytes of crushing origin from the Shimotsuburai fault of the Itoigawa-Shizuoka Tectonic Line active fault system, central Japan. *Jour. Geol. Soc. Japan* 110, 779–790. doi:10.5575/geosoc.110.779

Karato, S. (1989). Grain growth kinetics in olivine aggregates. *Tectonophysics* 168, 255–273. doi:10.1016/0040-1951(89)90221-7

Li, J.-P., O'Neill, H. S. C., and Seifert, F. (1995). *Subsolidus phase relations in the system MgO-S⅄ -Cr-0 in equilibrium with metallic Cr, and their significance for the petrochemistry of chromium.* 36.

Lin, A. (2008). *Fossil earthquakes: The formation and preservation of pseudotachylytes*. Berlin, Heidelberg: Springer Berlin Heidelberg. doi:10.1007/978-3-540-74236-4

Lin, A., and Shimamoto, T. (1998). Selective melting processes as inferred from experimentally generated pseudotachylytes. *Journal of Asian Earth Sciences* 16, 533–545. doi:10.1016/S0743-9547(98)00040-3

Lin, A., Takano, S., Hirono, T., and Kanagawa, K. (2013). Coseismic dehydration of serpentinite: evidence from high-velocity friction experiments. *Chemical Geology* 344, 50–62. doi:10.1016/j.chemgeo.2013.02.013

Lund, M. G., and Austrheim, H. (2003). High-pressure metamorphism and deep-crustal seismicity: evidence from contemporaneous formation of pseudotachylytes and eclogite facies coronas. *Tectonophysics* 372, 59–83. doi:10.1016/S0040-1951(03)00232-4

Magloughlin, J. F. (1992). Microstructural and chemical changes associated with cataclasis and frictional melting at shallow crustal levels: the cataclasite-pseudotachylyte connection. *Tectonophysics* 204, 243–260. doi:10.1016/0040-1951(92)90310-3

McKenzie, D., and Brune, J. N. (1972). Melting on fault planes during large earthquakes. *Geophysical Journal International* 29, 65–78. doi:10.1111/j.1365-246X.1972.tb06152.x

McNulty, B. A. (1995). Pseudotachylyte generated in the semi-brittle and brittle regimes, Bench Canyon shear zone, central Sierra Nevada. *Journal of Structural Geology* 17, 1507–1521. doi:10.1016/0191-8141(95)00052-F

Morgunova, A. A., and Perchuk, A. L. (2012). Petrology of precambrian metaultramafites of the gridino high-pressure complex (*karelia*). *Russian Geology and Geophysics* 53, 131–146. doi:10.1016/j.rgg.2011.12.011

Naemura, K., Hirajima, T., and Svojtka, M. (2009). The pressure–temperature path and the origin of phlogopite in spinel–garnet peridotites from the blanský les massif of the moldanubian zone, Czech republic. *Journal of Petrology* 50, 1795–1827. doi:10.1093/petrology/egp052

Obata, M., and Karato, S. (1995). Ultramafic pseudotachylite from the Balmuccia peridotite, Ivrea-Verbano zone, northern Italy. *Tectonophysics* 242, 313–328. doi:10.1016/0040-1951(94)00228-2

Piccardo, G. B., Ranalli, G., and Guarnieri, L. (2010). Seismogenic shear zones in the lithospheric mantle: ultramafic pseudotachylytes in the lanzo peridotite (western alps, nw italy). *Journal of Petrology* 51, 81–100. doi:10.1093/petrology/egp067

Ravna, E., Kullerud, K., and Ellingsen, E. (2006). Prograde garnet-bearing ultramafic rocks from the tromsø nappe, northern scandinavian Caledonides☆. *Lithos* 92, 336–356. doi:10.1016/j.lithos.2006.03.058

Rebay, G., Spalla, M. I., and Zanoni, D. (2012). Interaction of deformation and metamorphism during subduction and exhumation of hydrated oceanic mantle: insights from the western alps: deformation-metamorphism of hp serpentinites. *Journal of Metamorphic Geology* 30, 687–702. doi:10.1111/j.1525-1314.2012.00990.x

Robinson, P. T., Bai, W.-J., Malpas, J., Yang, J.-S., Zhou, M.-F., Fang, Q.-S., et al. (2004). Ultra-high pressure minerals in the Luobusa Ophiolite, Tibet, and their tectonic implications. *SP* 226, 247–271. doi:10.1144/GSL.SP.2004.226.01.14

Sibson, R. H. (1975). Generation of pseudotachylyte by ancient seismic faulting. *Geophys J Int* 43, 775–794. doi:10.1111/j.1365-246X.1975.tb06195.x

Spray, J. G. (1987). Artificial generation of pseudotachylyte using friction welding apparatus: simulation of melting on a fault plane. *Journal of Structural Geology* 9, 49–60. doi:10.1016/0191-8141(87)90043-5

Spray, J. G. (1995). Pseudotachylyte controversy: fact or friction? *Geol* 23, 1119. doi:10.1130/0091-7613(1995)023<1119:PCFOF>2.3.CO;2

Suzuki, A., (2001). Viscosity of komatiite magma at high pressure. Bayerishes Geoinstitut Annual Report Available at: http://www.bgi.uni-bayreuth.de/annual_report/navigat.php3?year=2001.

Swanson, M. T. (1992). Fault structure, wear mechanisms and rupture processes in pseudotachylyte generation. *Tectonophysics* 204, 223–242. doi:10.1016/0040-1951(92)90309-t

Trommsdorff, V., Sánchez-Vizcaíno, V. L., Gómez-Pugnaire, M. T., and Müntener, O. (1998). High pressure breakdown of antigorite to spinifex-textured olivine and orthopyroxene, SE Spain. *Contributions to Mineralogy and Petrology* 132, 139–148. doi:10.1007/s004100050412

Tullis, J., and Yund, R. A. (1982). Grain growth kinetics of quartz and calcite aggregates. *The Journal of Geology* 90, 301–318. doi:10.1086/628681

Ueda, T., Obata, M., Di Toro, G., Kanagawa, K., and Ozawa, K. (2008). Mantle earthquakes frozen in mylonitized ultramafic pseudotachylytes of spinel-lherzolite facies. *Geol* 36, 607. doi:10.1130/G24739A.1

Whitney, D. L., and Evans, B. W. (2010). Abbreviations for names of rock-forming minerals. *American Mineralogist* 95, 185–187. doi:10.2138/am.2010.3371

Wu, F.-Y., Liu, C.-Z., Zhang, L.-L., Zhang, C., Wang, J.-G., Ji, W.-Q., et al. (2014). Yarlung Zangbo ophiolite:A critical updated view. *Acta Petrol Sinica (in Chinese with English abstract)* 30, 293–325. doi:10.3986/AGS48106

Yang, J.-J., Fan, Z.-F., Yu, C., and Yan, R. (2014a). Coseismic formation of eclogite facies cataclasite dykes at Yangkou in the Chinese Su-Lu UHP metamorphic belt. *J. Meta. Geol.* 32, 937–960. doi:10.1111/jmg.12101

Yang, J.-J., Huang, M.-X., and Naemura, K. (2013). Towards a law for the metamorphic evolution of mantle-derived orogenic peridotites. *Acta Petrologica Sinica (in Chinese with English abstract)* 29 (5), 1479–1485.

Yang, J.-J., Huang, M.-X., Wu, Q.-Y., and Zhang, H.-R. (2014b). Coesite-bearing eclogite breccia: implication for coseismic ultrahigh-pressure metamorphism and the rate of the process. *Contrib Mineral Petrol* 167, 1013. doi:10.1007/s00410-014-1013-7

Yang, J.-J., and Powell, R. (2008). Ultrahigh-pressure garnet peridotites from the devolatilization of sea-floor hydrated ultramafic rocks. *Journal of Metamorphic Geology* 26, 695–716. doi:10.1111/j.1525-1314.2008.00780.x

Yang, J.-J. (2003). Relict edenite in a garnet lherzolite from the Chinese Su.Lu UHP metamorphic terrane: implications for metamorphic history. *American Mineralogist* 88, 180–188. doi:10.2138/am-2003-0121

Yang, J.-J., Zhang, H.-R., Chen, A.-P., and Huang, M.-X. (2016). Petrological evidence for shock-induced high- *P* metamorphism in a gabbro. *J. Metamorph. Geol.* 35, 121–140. doi:10.1111/jmg.12223

Zhang, H.-Y., Ba, D.-Z., Guo, T.-Y., Mo, X.-X., Xue, Y.-Z., Ruan, G.-F., et al. (1996). *Study of Luobusha typical chromite ore deposit Qusong county (in Chinese)*. Tibet (Xizang), Lhasa: Xizang People Press, 1–181.

Zhou, M.-F., Robinson, P. T., Malpas, J., and Li, Z. (1996). Podiform chromitites in the Luobusa ophiolite (southern Tibet): implications for melt-rock interaction and chromite segregation in the upper mantle. *J Petrology* 37, 3–21. doi:10.1093/petrology/37.1.3